Influence of local-field corrections on Thomson scattering in collision-dominated two-component plasmas

Carsten Fortmann,[1,2,*] August Wierling,[1] and Gerd Röpke[1]
[1]*Institut für Physik, Universität Rostock, 18051 Rostock, Germany*
[2]*Department of Physics and Astronomy, University of California Los Angeles, Los Angeles, California 90095, USA*
(Received 19 August 2009; revised manuscript received 26 January 2010; published 18 February 2010)

The dynamic structure factor, which determines the Thomson scattering spectrum, is calculated via an extended Mermin approach. It incorporates the dynamical collision frequency as well as the local-field correction factor. This allows to study systematically the impact of electron-ion collisions as well as electron-electron correlations due to degeneracy and short-range interaction on the characteristics of the Thomson scattering signal. As such, the plasmon dispersion and damping width is calculated for a two-component plasma, where the electron subsystem is completely degenerate. Strong deviations of the plasmon resonance position due to the electron-electron correlations are observed at increasing Brueckner parameters r_s. These results are of paramount importance for the interpretation of collective Thomson scattering spectra, as the determination of the free electron density from the plasmon resonance position requires a precise theory of the plasmon dispersion. Implications due to different approximations for the electron-electron correlation, i.e., different forms of the one-component local-field correction, are discussed.

DOI: 10.1103/PhysRevE.81.026405 PACS number(s): 51.70.+f, 52.25.Tx, 52.70.La

I. INTRODUCTION

Recently, Thomson scattering has been established as a diagnostic tool for high energy laser-matter interaction in particular for warm dense matter [1–5]. The Thomson signal probes the dynamic structure factor $S_{ee}(k,\omega)$ of the plasma [6]. Reversing the argument, we can synthesize the Thomson signal by using an appropriate expression for the dynamic structure factor, or equivalently the dielectric function of the plasma, and infer density and temperature conditions by matching the synthesized signal to the experimental one [7]. This technique has become a primary diagnostic tool for inertial confinement fusion projects, laboratory astrophysics, and laser generated warm dense matter in general. At such extreme conditions as present in the aforementioned examples, collisions and correlations have to be accounted for in modeling the Thomson scattering signal, i.e., $S_{ee}(k,\omega)$ [8].

Collective Thomson scattering, where photons scatter inelastically on the collective resonances of the plasma (plasmons) is well adapted for the diagnostics of plasmas at or near solid density using x-ray sources, since the plasmon peak is energetically well separated from the elastically scattered photons [9]. Measuring the plasmon resonance position allows for the direct determination of the free electron density provided the plasmon dispersion relation is known precisely, i.e., the relation between the resonance energy, the scattering wave vector at given temperature, density, and degree of ionization. The electron temperature can be inferred due to detailed balance from the ratio of the peak heights of the red and blue shifted plasmon, respectively [10].

In a proof-of-principle experiment, Glenzer *et al.* [4] have demonstrated plasmon scattering in warm dense matter. Fitting of the plasmon signal by random phase approximation (RPA) overestimated the plasma temperature as compared to simulations. This indicated that additional plasmon damping due to collisions needed to be taken into account. To this end, the Born-Mermin (BM) approach was successfully applied.

The principal difficulty in describing the plasmon dispersion as well as the plasmon damping consistently, is the following: the plasmon dispersion is contained already in the collisionless theory, i.e., the RPA. On the other hand, tractable models of plasmon damping, such as the Drude model, are only strictly valid in the long-wavelength limit, i.e., $k \to 0$. The Mermin approximation [11] has been found [12] to be a useful way of bridging between the collision-less plasma (RPA) at large wave vectors, where collisions may be neglected due to strong Landau damping, and collisions in the long-wavelength limit, i.e., a Drude-like expression for the dielectric function. However, in the static limit $\omega \to 0$, the Mermin dielectric function equals the RPA expression, i.e., static correlations (at finite k) beyond RPA are not incorporated in the Mermin approach. These static correlations can be described, e.g., via the local-field correction (LFC) factor [13]. An extension of the conventional Mermin approach, that incorporates both static local-field corrections and the dynamical electron-ion collision frequency has been suggested in Ref. [14] using the Zubarev approach to the nonequilibrium statistical operator [15,16]. This scheme guarantees the correct account of electron correlations in the static limit.

Starting from this extended Mermin ansatz, a systematic study of the influence of both electron-ion collisions as well as electron-electron correlations on the Thomson scattering is now possible. It is the objective of this paper to contribute to such a study. In particular, since the correct form of the dynamic as well as the static local-field corrections for the interacting electron gas is still a matter of debate, we compare a few recent suggestions in their consequences for the Thomson scattering signal. It should be noted that the influence of local-field corrections on the elastic part of the scattering spectrum, the so-called ion feature, has been studied

*fortmann1@llnl.gov

by Gregori and co-workers [17,18]. Here, we focus on the inelastically scattered light due to plasmon excitation.

The paper is organized as follows: in Sec. II, we give a brief review of the formalism and the approach to the dynamic collision frequency. Section III in some detail explains the different models for the dynamic local-field correction considered here. Results for the plasmon dispersion and damping are discussed in Sec. IV. Finally, conclusions and an outlook complete this paper.

II. THEORETICAL BACKGROUND

We consider a neutral plasma of electrons and ions in thermal equilibrium with electron density n_e, ion density $n_i = n_e$ (i.e., $Z=1$) and temperature T. For later use, we introduce the Fermi wave vector $k_F=(3\pi^2 n_e)^{1/3}$, the Fermi energy $E_F=\hbar^2 k_F^2/(2m_e)$, and the Brueckner parameter r_s given by $(4\pi/3)n_e a_B^3 r_s^3=1$, where a_B is Bohr's radius. These parameters are relevant in our context, because we use the model of an electron gas at $T=0$ interacting with an inert background of ions in carrying out our exploratory calculations. In particular, the coupling parameter Γ, i.e., the ratio of average potential energy per particle to average kinetic energy per particle, scales as $\propto r_s$ in Fermi degenerate plasmas, $\Gamma \simeq 0.5 r_s$. As a consequence, the electron-electron coupling decreases with increasing electron density and the theory of ideal Fermi gases is recovered in the limiting case of $n_e \to \infty$. This is in marked contrast to the case of classical plasmas, where $\Gamma \propto n_e^{1/3}$.

A. Thomson scattering and Born-Mermin approach

It is well-known, see [3–5], that the experimental Thomson scattering cross section is related to the dynamic structure factor of all electrons in the plasma according to

$$\frac{d^2\sigma}{d\Omega d\omega} = \sigma_T \frac{k_1}{k_0} S_{ee}(k,\omega). \tag{1}$$

In this expression, $\sigma_T=6.65\times10^{-29}$ m^2 is the Thomson cross section, and k_0 and k_1 are the wave numbers of the incident and the scattered light. The energy and momentum transfer are given by $\Delta E=\hbar\omega=\hbar\omega_1-\hbar\omega_0$ and $\hbar\mathbf{k}=\hbar\mathbf{k}_1-\hbar\mathbf{k}_0$. The momentum is related to the scattering angle θ_s in the limit $\hbar\omega \ll \hbar\omega_0$ by $k=4\pi\sin(\theta_s/2)/\lambda_0$ for an incident wavelength λ_0. Here, we follow Chihara' s approach [6], in that the total dynamic structure factor can be written in terms of contributions from free electrons and bound electrons. In this paper, only the dynamic structure factor of free electrons is considered.

In thermodynamic equilibrium, the dynamic structure factor $S_{ee}(k,\omega)$ and the longitudinal response function $\chi_{ee}(k,\omega)$ are related via the fluctuation-dissipation theorem

$$S_{ee}(k,\omega) = -\frac{1}{\pi n_e}\frac{1}{1-e^{-\hbar\omega/(k_B T)}}\mathrm{Im}\,\chi_{ee}(k,\omega). \tag{2}$$

Theoretical approaches to the dynamic structure factor of two-component plasmas have been developed starting from different approaches such as perturbation theory, the viscoelastic model [19], the recurrence-relation method [20], or the moment approach, see Ref. [21]. As an example for a perturbative treatment, we mention Refs. [22,23]. There, based on the generalized linear response theory of Zubarev, a systematic account of correlations as well as collisions has been accomplished by partial summation of diagram classes using thermodynamic Green's functions. While a detailed evaluation of the resulting expressions for the response functions is cumbersome at arbitrary wave vectors k, numerical calculations have been carried out in the long-wavelength limit $k \to 0$. In particular, approximative expressions for the collision frequency $\nu(\omega)$ have been studied taking care of strong collisions as well as dynamical screening in a consistent manner.

To generate approximative results for the response function at finite wave vectors k, we follow an idea suggested by Mermin [11]. Ensuring particle number conservation by introducing local thermal equilibrium together with a relaxation time ansatz, the electron-electron response function is approximated by

$$\chi_{ee}^{(M)}(k,\omega) = \left(1-\frac{i\omega}{\eta}\right)\frac{\chi_{ee}^{\mathrm{RPA}}(k,\omega+i\eta)\chi_{ee}^{\mathrm{RPA}}(k,0)}{\chi_{ee}^{\mathrm{RPA}}(k,\omega+i\eta)-\frac{i\omega}{\eta}\chi_{ee}^{\mathrm{RPA}}(k,0)}, \tag{3}$$

with a relaxation parameter η. For details, see Ref. [16]. Here, χ_{ee}^{RPA} is the electron response function in random phase approximation, i.e.,

$$\chi_{ee}^{\mathrm{RPA}}(k,\omega) = \frac{\chi_e^{(0)}(k,\omega)}{1-V(k)\chi_e^{(0)}(k,\omega)}, \tag{4}$$

where $\chi_e^{(0)}(k,\omega)$ is the ideal, i.e., noninteracting response function, see [24]. For $T=0$, this ideal response can be found as

$$V(k)\chi_e^{(0)}(k,\omega) = -\frac{\chi_0^2}{4z^3}[g(u+z)-g(u-z)], \tag{5}$$

with $u=m\omega/(\hbar k k_F)$, $z=k/(2k_F)$, $\chi_0^2=(\pi k_F a_B)^{-1}$ and

$$g(x) = x+\frac{1}{2}(1-x^2)\ln\frac{x+1}{x-1}, \tag{6}$$

The function $g(x)$ given here is a generalization of the function $g(x)$ given in [24] to complex arguments. Furthermore, $V(k)=e^2/(\epsilon_0 k^2 \Omega_0)$ denotes the Coulomb potential in momentum space, with the normalization volume Ω_0. Note, that Eq. (3) reduces to the RPA expression in the absence of collisions, i.e., $\eta=0$. Also, in the long-wavelength limit, Eq. (3) turns into the familiar Drude form, allowing to identify the relaxation parameter η as the collision frequency $\eta=\nu(\omega)$. For practical calculations, the collision frequency is evaluated in Born approximation, which will be discussed in more detail in Sec. II C.

The Born-Mermin approach, i.e., the combination of the Mermin ansatz for the response function (3) and the Born approximation for the collision frequency, allows for the consistent interpretation of x-ray Thomson scattering in warm dense matter [4]. On the other hand, there are certain

deficiencies associated to the Born-Mermin approach. Namely, electron-electron correlations, which become important at lower temperatures due to the Fermi degeneracy, are not contained. It is well-known [26] that electron-electron correlations lead to severe modifications of the plasmon dispersion at wave numbers k in the vicinity of the Fermi wave number k_F. In order to account for both electron-electron correlations as well as electron-ion collisions in a unified, consistent approach, an extended Mermin approach has been suggested [14], which will be outlined briefly in the next section.

B. Extended Mermin approach

To account for correlations among the electrons, an extension of the traditional Mermin expression has been suggested, see Ref. [14]. For an adiabatic model with inert ions, it reduces to replacing the RPA response function in Eq. (3) by the response function of the interacting one-component (OCP) electron gas $\chi_{ee}^{\mathrm{OCP}}(k,\omega)$,

$$\chi_{ee}^{(\mathrm{xM})}(k,\omega) = \left[1 - \frac{i\omega}{\nu(\omega)}\right] \times \left\{ \frac{\chi_{ee}^{\mathrm{OCP}}[k,\omega + i\nu(\omega)]\chi_{ee}^{\mathrm{OCP}}(k,0)}{\chi_{ee}^{\mathrm{OCP}}[k,\omega + i\nu(\omega)] - [i\omega/\nu(\omega)]\chi_{ee}^{\mathrm{OCP}}(k,0)} \right\}, \tag{7}$$

where the label xM indicates the extended Mermin expression for the response function. Note, that the same expression has been derived independently by Barriga-Carrasco [25]. Traditionally, the OCP response function is represented using a dynamic local-field correction $G_{ee}(k,\omega)$ as

$$\chi_{ee}^{\mathrm{OCP}}(k,\omega) = \frac{\chi_e^{(0)}(k,\omega)}{1 - V(k)[1 - G_{ee}(k,\omega)]\chi_e^{(0)}(k,\omega)}. \tag{8}$$

Having a collisionless plasma $\nu(\omega)=0$, the response function is solely the OCP expression. Due to the fact, that electron-electron collisions do not contribute in the long-wavelength limit, i.e., $G_{ee}(k,\omega) \propto k^2$ for $k \to 0$, this expression still reduces to the Drude-like form for small k with the same $\nu(\omega)$ as before. However, contrary to Eq. (3), the static limit is now given by the electron-electron correlation in the OCP,

$$\lim_{\omega \to 0} \chi_{ee}^{(\mathrm{xM})}(k,\omega) = \chi_{ee}^{\mathrm{OCP}}(k,0). \tag{9}$$

C. Collision frequency at arbitrary degeneracy

For the exploratory calculation discussed here, we use the collision frequency in Born approximation and for arbitrary degeneracy, see Ref. [23],

$$\mathrm{Re}\ \nu(\omega) = \frac{\epsilon_0 n_i \Omega_0^2}{6\pi^2 e^2 n_e m_e} \int_0^\infty dq q^6 V_S(q)^2 S_i(q) \frac{1}{\omega} \mathrm{Im}\ \epsilon_{\mathrm{RPA,e}}(q,\omega), \tag{10}$$

where $V_S(q) = V(q)/\epsilon_{\mathrm{RPA,e}}(q,0)$ is the statically screened potential, $S_i(q)$ is the static structure factor of the ions, which can be taken, e.g., from HNC calculations or from MD simulations. In this work, we used $S_i(q) \equiv 1$ in order not to mix different contributions and to keep the discussion of our results as straightforward as possible. Typically, the collision frequency is lowered if the ion structure is taken into account. Furthermore, $\epsilon_{\mathrm{RPA,e}}(q,\omega) = 1 - V(q)\chi_e^{(0)}(q,\omega)$ is the dielectric function of the electron OCP. Again, we determine the RPA dielectric function for $T=0$ by using Eq. (5).

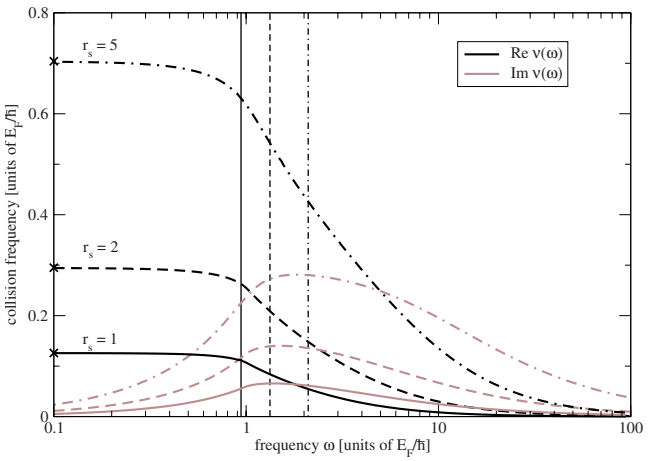

FIG. 1. (Color online) Real (black curves) and imaginary part (gray curves) of the collision frequency $\nu(\omega)$ as a function of the frequency ω. Various values of the Brueckner parameter r_s are considered. The thin lines indicate the position of the plasma frequency ω_{pl} for $r_s=1$ (solid), $r_s=2$ (dashed), and $r_s=5$ (dash-dotted). Crosses at $\omega = 0.1 E_F/\hbar$ indicate the static limit for the collision frequency (Ziman formula). The vertical lines give the plasma frequency ω_{pl}.

We restrict ourselves to the Born approximation (10) since we want to focus on the interplay between collisions and electron-electron correlations and the role of different approximations for the OCP local-field corrections. More advanced expressions are given in Ref. [23]. Calculations beyond the Born approximation should include electron-electron effects on the collision frequency, which can be taken into account by increasing the number of moments in the linear response approach, see Ref. [23] as well.

In Fig. 1, we show the collision frequency $\nu(\omega)$ as a function of the frequency ω for three different values of the Brueckner parameter $r_s = 1, 2, 5$ and at $T=0$. Here and in the following, we choose $Z=1$. As a reference, we also show the position of the plasma frequency $\omega_{\mathrm{pl}} = (n_e e^2/\epsilon_0 m_e)^{1/2}$ as thin vertical lines for the three cases. Note that the fact that $\hbar\omega_{\mathrm{pl}}/E_F \simeq 1$ for $r_s=1$ is purely fortuitous, since $\hbar\omega_{\mathrm{pl}}/E_F \simeq 0.9405\sqrt{r_s}$.

The imaginary part of the collision frequency Im $\nu(\omega)$ is connected to Re $\nu(\omega)$ by a Kramers-Kronig relation

$$\mathrm{Im}\ \nu(\omega) = \int_{-\infty}^{\infty} \frac{d\omega'}{\pi} \frac{\mathrm{Re}\ \nu(\omega')}{\omega - \omega'}. \tag{11}$$

The account of this imaginary part is essential for obeying both, the f-sum rule and the perfect screening sum rule. While, loosely speaking, the real part of $\nu(\omega)$ leads to a broadening of the plasmon at $k=0$, the imaginary part produces a shift in the plasmon. For a static frequency $\omega=0$, the

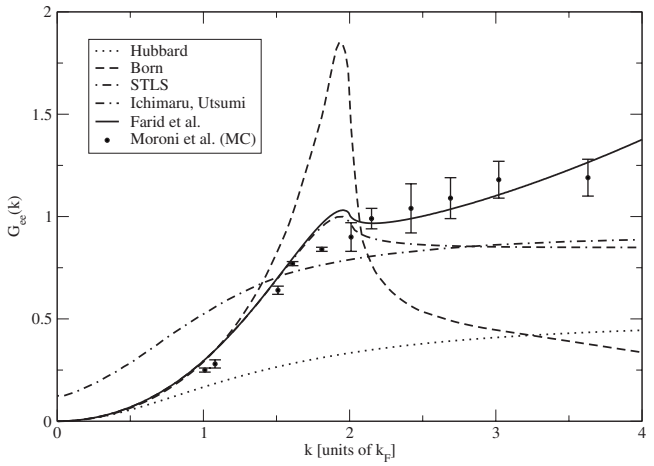

FIG. 2. Static local-field correction $G_{ee}(k)$ for $r_s=2$. Approximations: Hubbard (dotted), Born (dashed), Singwi-Tosi-Land-Sjoelander (STLS) (dash-dotted), Utsumi and Ichimaru (dash-dash-dotted), Farid *et al.* (solid), and Moroni *et al.* (points with error bars).

imaginary part vanishes, i.e., replacing the dynamic by a static collision frequency $\nu(0)$ one ignores the shift in the plasmon position. As a reference, the crosses at $\omega=0.1E_F/\hbar$ indicate the value of $\nu(0)=\mathrm{Re}\ \nu(0)$ as given by the Ziman formula evaluated in Born approximation [22],

$$\frac{\hbar\nu^{(\mathrm{Ziman})}}{E_F}=0.11523r_s^2\left[\ln\left(1+\frac{6.02921}{r_s}\right)-\frac{1}{1+r_s/6.02921}\right]. \tag{12}$$

Note that the collision frequency increases with increasing r_s, i.e., with increasing electron-electron coupling, but with decreasing electron density.

III. LOCAL-FIELD CORRECTIONS FOR AN INTERACTING ELECTRON GAS AT $T=0$

A. Static local-field correction for the OCP

In an often used approximation, the dynamics in the local-field correction is ignored, reducing it to the static limit only,

$$\chi_{ee}^{\mathrm{OCP}}(k,\omega)=\frac{\chi_e^{(0)}(k,\omega)}{1-V(k)[1-G_{ee}(k)]\chi_e^{(0)}(k,\omega)}. \tag{13}$$

For the static local-field correction $G_{ee}(k)$, a plethora of approximations have been suggested beginning with the original paper by Hubbard [13]. Here, it is impossible to give an exhaustive review. For an overview of other approximations, see Ref. [28]. For the sake of illustration, we compare a few approximations in Fig. 2 for $r_s=2$. Besides Hubbard's approximation shown as dotted curve, we also give the Singwi-Tosi-Land-Sjølander approximation [30] (dash-dotted curve), the widely used result by Utsumi and Ichimaru [26] (dash-dash-dotted curve), the extension of the latter given by Farid *et al.* [27] (solid curve), as well as the Born approximation [29] (dashed curve). Note that the latter exhibits a sharp resonance at $k=2k_F$, which is an artifact due to the discontinuity of the Fermi distribution function at k_F and occurs for all r_s. For comparison and to evaluate the aforementioned analytic expressions, we also show the Monte Carlo (MC) simulation data by Moroni *et al.* [31] (points with error bars). Qualitatively similar results are obtained for other values of r_s. For small values of k, the Utsumi-Ichimaru approximation and the extended model of Farid *et al.* are identical by construction $\lim_{k\to 0}G_{\mathrm{UI}}(k)=\lim_{k\to 0}G_{\mathrm{Farid}}(k)=\gamma_0(r_s)k^2/k_F^2$. Here, $\gamma_0(r_s)$ is an exactly known function of the correlation energy, ensuring the compressibility sum rule [26]. There is a good agreement with the MC data and both, the Utsumi-Ichimaru and the Farid *et al.* description, while the other approximations do not describe these so well. In the deep inelastic regime at large k, Farid *et al.* take account of the results by Holas [32], that $G_{ee}(k)$ scales as k^2, i.e.,

$$\lim_{k\to\infty}G_{ee}^{\mathrm{Farid}}(k)=\frac{2}{3}[1-g(0)]+\frac{48E_F^2}{35\hbar^2\omega_{\mathrm{pl}}^2}\delta_4-\frac{16E_F^2}{25\hbar^2\omega_{\mathrm{pl}}^2}(2\delta_2+\delta_2^2)+\frac{4E_F^2}{5\hbar^2\omega_{\mathrm{pl}}^2}\delta_2\frac{k^2}{k_F^2}, \tag{14}$$

with δ_2 and δ_4 being constants only depending on r_s, and $g(r)$ the radial pair distribution function. The k^2 asymptotics is not included into the Utsumi-Ichimaru ansatz, where

$$\lim_{k\to\infty}G_{ee}^{\mathrm{UI}}(k)=\frac{2}{3}[1-g(0)]. \tag{15}$$

Within error bars, the MC data support the quadratic scaling. For our discussion, this difference is rather unimportant, since the plasmon ceases to be a well-defined mode already at momenta smaller than k_F, while the differences between Utsumi-Itchimaru and Farid *et al.* arise for $k\gtrsim 2k_F$.

B. Dynamic local-field corrections for the OCP

As already mentioned, there are several approximative approaches to the dynamic structure factor of the electron gas. Here, we describe the approach of Dabrowski [33] and the approach of Hong and Lee [34]. Both approaches are interpolation schemes incorporating sum rules and other exact properties. In particular, the static properties are inputs into these schemes and we can use the local-field correction of Farid *et al.* again in this case. This would have been impossible if we choose perturbative results of, e.g., Richardson and Ashcroft [35].

Being a dynamical quantity, the local-field correction is also a complex quantity obeying Kramers-Kronig like relations. For the real part $\mathrm{Re}\ G_{ee}(k,\omega)$ of the dynamic local-field correction, the static limit is just approximated by $G_{ee}(k)$ given above. The high-frequency asymptotics is given by the third-frequency moment sum rule and therefore by the static structure factor and the correlated kinetic energy of the electron gas, see Refs. [36,37],

$$\lim_{\omega\to\infty}\mathrm{Re}\ G_{ee}(k,\omega)=I(k)-\frac{2k^2}{m\omega_{\mathrm{pl}}^2}(\langle E_{\mathrm{kin}}\rangle-\langle E_{\mathrm{kin}}\rangle_0), \tag{16}$$

where $I(k)$ in turn is given by the static OCP structure factor $S(k)$

$$I(k) = -\frac{1}{N}\sum_{\vec{q}\neq\vec{k},\vec{0}} K(\vec{k},\vec{q})(\vec{k}\cdot\vec{q})^2[S(|\vec{q}-\vec{k}|)-1], \quad (17)$$

and

$$K(\vec{k},\vec{q}) = \frac{\vec{q}\cdot\vec{k}}{k^2} + \frac{\vec{q}\cdot(\vec{q}-\vec{k})}{|\vec{q}-\vec{k}|^2}. \quad (18)$$

Furthermore, $\langle E_{\mathrm{kin}}\rangle$ is the kinetic energy of the interacting electron gas, $\langle E_{\mathrm{kin}}\rangle_0$ its noninteracting counterpart.

Dabrowski also incorporates the perturbative result of Glick and Long [38] for the high-frequency behavior of the imaginary part of the dynamic structure factor. He extends a Padé approximation suggested by Gross and Kohn [39] to finite values of the wave vector,

$$\mathrm{Im}\, G_{ee}(k,\omega) = \frac{a(k)\omega}{(1+b(k)\omega^2)^{5/4}}, \quad (19)$$

with

$$a(k) = Ck^2\left(\frac{\mathrm{Re}\, G_{ee}(k,0) - \mathrm{Re}\, G_{ee}(k,\infty)}{CDk^2}\right)^{5/3}, \quad (20)$$

$$b(k) = \left(\frac{\mathrm{Re}\, G_{ee}(k,0) - \mathrm{Re}\, G_{ee}(k,\infty)}{CDk^2}\right)^{4/3}, \quad (21)$$

and $C=23/60\alpha r_s$, $D=\Gamma(3/4)/[\sqrt{\pi}\Gamma(5/4)]\approx 0.763$, $\alpha=[4/(9\pi)]^{1/3}$. The corresponding real part is then obtained by a Kramers-Kronig relation,

$$\mathrm{Re}\, G_{ee}(k,\omega) = \mathrm{Re}\, G_{ee}(k,\infty) + P\int_{-\infty}^{\infty}\frac{d\omega'}{\pi}\frac{\mathrm{Im}\, G_{ee}(k,\omega')}{\omega'-\omega}, \quad (22)$$

where $P\int$ indicates Cauchy principal value integration.

As a second option for the dynamic local-field correction of the OCP we mention the approach of Hong and Lee [34,36], which is based on the recurrence-relation technique. Specifically, we use the lowest dynamical extension of the local-field correction, which can be introduced by this technique. Adapting the notation to the present paper, the dynamical local-field correction reads

$$G_{ee}(k,z) = G_{ee}(k,0) + [G_{ee}(k,\infty) - G_{ee}(k,0)]c_2^0(z) \quad (23)$$

with a function c_2^0 given by [40]

$$c_2^0(z) = \frac{\Delta_1^0}{\Delta_2^0}\left(\frac{\chi^{(0)}(k,0)}{\chi^{(0)}(k,z)} - 1\right) + \frac{z^2}{\Delta_2^0}. \quad (24)$$

Here, the quantities Δ_1^0 and Δ_2^0 are the ideal recurrants

$$\Delta_1^0 = -\frac{\omega_{\mathrm{pl}}^2}{V(k)\chi_e^{(0)}(k)}, \quad \Delta_2^0 = \left[\frac{12}{5}\left(\frac{k}{k_F}\right)^2 + \left(\frac{k}{k_F}\right)^4\right]\left(\frac{E_F}{\hbar}\right)^2 - \Delta_1^0 \quad (25)$$

Both approaches have been adapted in the present work to the most recent results for the static OCP electron-electron structure factor $S(k)$ and the correlated kinetic energy, see Ref. [41].

IV. COMPARISON OF DIFFERENT APPROXIMATIONS

Instead of showing the dynamical structure factor $S_{ee}(k,\omega)$ for each of the different approximations and for various values of the wave vector k and the frequency ω, we introduce the plasmon position $\omega(k)$ as the position of the maximum in the dynamical structure factor and the plasmon width $\Gamma(k)$ as the full width at half maximum (FWHM) of $S_{ee}(k,\omega)$. In a collision-less plasma at $T=0$, the plasmon is a well-defined mode for $k<k_0(r_s)$ corresponding to a δ-like spike in the dynamic structure factor. Its position is given by the solution of $V(k)\chi^{(0)}[k,\omega(k)]=1$. For small k, $\omega(k)$ can be approximated by the Gross-Bohm relation

$$\left(\frac{\omega_{\mathrm{GB}}(k)}{E_F}\right)^2 = \left(\frac{\omega_{\mathrm{pl}}}{E_F}\right)^2 + \frac{12}{5}\left(\frac{k}{k_F}\right)^2. \quad (26)$$

For $k>k_0(r_s)$, Landau damping sets in, i.e., electrons in the Fermi sea take energy (momentum) from the collective mode. This process is not possible at smaller momenta since the final momentum still lies inside the Fermi sphere [24]. The wave vector $k_0(r_s)$, where Landau damping sets in, can be estimated as the intersection of the Gross-Bohm relation (26) and the single-particle ridge, i.e., k_0 is the solution of $\omega_{\mathrm{GB}}(k_0)=\hbar(k_0^2+2k_0k_F)/2m_e$. For small r_s, one obtains $k_0(r_s)/k_F\simeq 0.9405\sqrt{r_s}/2$ [28]. Evaluation of the full RPA response function yields $k_0(r_s)=0.53k_F$, $0.72k_F$, and $0.99k_F$ for the values $r_s=1$, 2, and 5, respectively, following the $\sqrt{r_s}$ scaling roughly. Deviations are due to the Gross-Bohm relation being limited to small r_s.

Collisions as well as correlations modify these RPA dispersion relations leading to a shift and a broadening of the plasmon even at $k<k_0(r_s)$.

A. Plasmon dispersion without collisions

In a first step, we discuss the effects induced only by local-field corrections, i.e., for $\nu(\omega)=0$. The modifications of the plasmon properties are shown in Fig. 3 for $r_s=1$ and in Fig. 4 for $r_s=5$. RPA (dotted), static local-field corrections (dashed) and dynamic local fields (solid) given by the improved Dabrowski interpolation scheme are compared. Furthermore, we also show the Gross-Bohm dispersion relation (26). Here and in the following figures, black lines indicate the plasmon position, whereas gray lines give the plasmon damping width.

All dispersion curves start at the same origin, e.g., the plasma frequency (note again that $\hbar\omega_{\mathrm{pl}}/E_F=0.9405\sqrt{r_s}$). At increasing k, deviations of the LFC curves from the RPA behavior are observed, reflecting the k^2 scaling of the LFC at small k. In the case of static LFC corrections, these deviations are quite small. Also, the dynamic LFC is only a minor correction to the static expression. This is consistent with the plasmon width, which is below 1% for almost all wave vectors k. Note that the rapid increase above $0.55k_F$ is due to the onset of Landau damping in the RPA expression. The Gross-Bohm relation works well except for $k\gtrsim 0.3k_F$, i.e., close to k_0.

For $r_s=5$, more noticeable deviations occur. Also, a clear influence of dynamical LFC is visible. This is also reflected

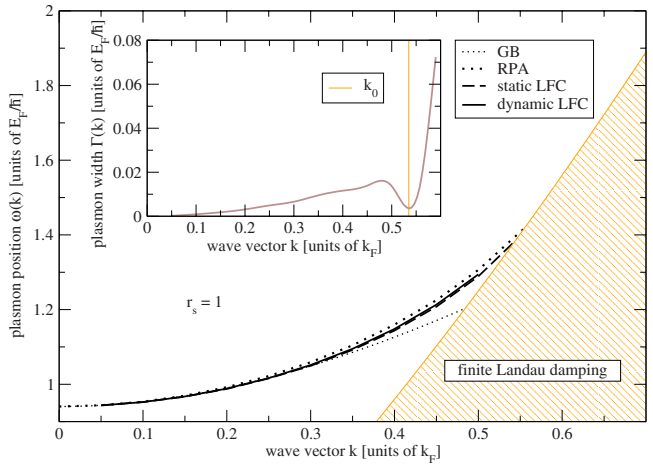

FIG. 3. (Color online) Plasmon shift $\omega(k)$ and plasmon width $\Gamma(k)$ as a function of the wave vector k for $r_s=1$. We compare the static local-field correction (dashed) to the dynamic local-field correction (solid). Dotted curve: RPA, thin dotted curve: Gross-Bohm approximation. No collisions are included. The (yellow) hatched area indicates the range of finite Landau damping.

in the plasmon damping, where a width of up to 17% is found, see inset in Figs. 3 and 4, where the plasmon damping width using the dynamical LFC is shown. The dip in the plasmon width at k_0 is due the imaginary part of the LFC at this position, which has a minimum here due to its construction. We interpret it as an artifact of the approximation with no physical relevance. The Gross-Bohm relation gives a good approximation to the RPA dispersion again up to $k \simeq 0.3k_F$, however since here $k_0=0.99k_F$, it is not capable to describe the plasmon dispersion up to the onset of Landau damping. This shows the limitations of the Gross-Bohm relation.

B. Results for the extended Mermin approach

We start the presentation of the results for the extended Born-Mermin approach by focusing on the long-wavelength

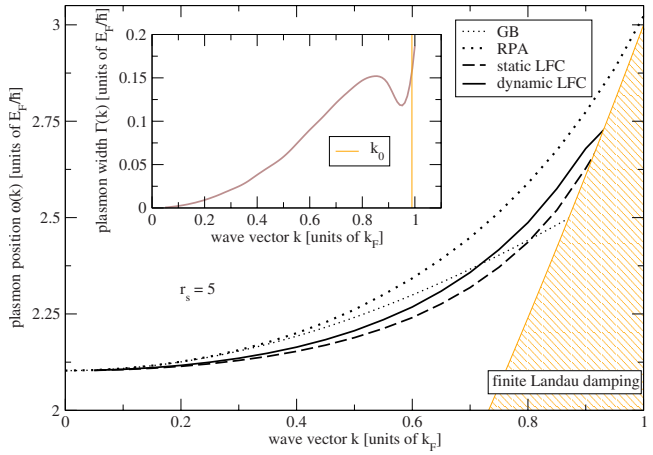

FIG. 4. (Color online) Plasmon shift $\omega(k)$ and plasmon width $\Gamma(k)$ as a function of the wave vector k for $r_s=5$. Dashed: static local-field correction, solid: dynamic local-field correction. Dotted: RPA, thin dotted: Gross-Bohm approximation. No collisions are included.

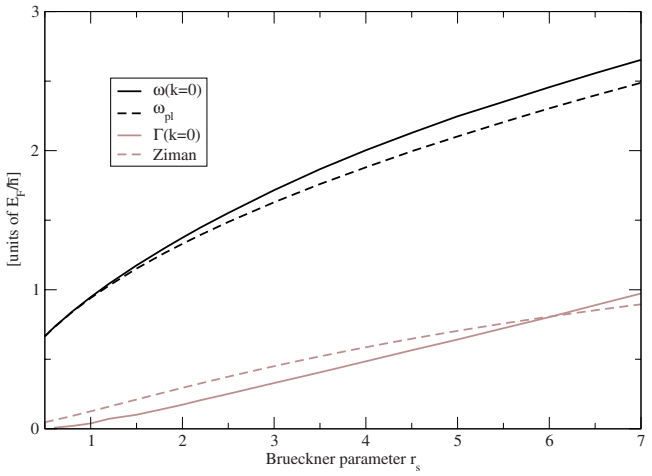

FIG. 5. (Color online) Plasmon shift $\omega(k=0)$ (solid black) and width $\Gamma(k=0)$ (solid gray) as a function of the Brueckner parameter r_s. Here, we account for electron-ion collisions using only the traditional Born-Mermin approximation. No local-field corrections are considered. Dashed black: plasma frequency $\omega_{\rm pl}/E_F \propto \sqrt{r_s}$, dashed gray: Ziman collision frequency.

limit $k \to 0$. In this limit, the Born-Mermin ansatz reduces to a Drude-type dielectric function with a frequency-dependent and complex collision frequency $\nu(\omega)$. This frequency leads to a broadening and a shift in the plasmon as can be seen from the imaginary part of the inverse dielectric function, which is given by

$$\text{Im}\ \epsilon^{-1}(k \to 0, \omega) = -\frac{\text{Re}\ \nu(\omega)\omega\omega_{\rm pl}^2}{[\omega^2 - \omega_{\rm pl}^2 - \text{Im}\ \nu(\omega)\omega]^2 + [\text{Re}\ \nu(\omega)]^2\omega^2}. \quad (27)$$

To zeroth order, the real part of the collision frequency is connected to a broadening, while the imaginary part induces a shift in the plasmon. Local-field corrections do not play any role in this limit as discussed above. The shift and the broadening are illustrated in Fig. 5 as a function of the Brueckner parameter r_s. Note, that both width and position are scaled by the $E_F \propto r_s^{-2}$. At small $r_s (r_s < 5)$, the width (solid gray curve) evolves parallel to the Ziman formula (12), given as dashed gray curve. The offset follows from the fact that the damping width $\Gamma(0) \simeq \text{Re}\ \nu(\omega_{\rm pl})$ is smaller than the Ziman limit $\nu(0)$, due to the decrease of Re $\nu(\omega)$ with increasing ω. At higher r_s (approaching $r_s=6$), the Ziman formula bends downwards due to the second term in Eq. (12), whereas the observed plasmon damping width keeps rising as expected at increased coupling r_s. This is partly due to the contribution of Im $\nu(\omega)$ to the plasmon damping, which becomes important at increased r_s. However, here and in the following, we limit our discussion to $r_s \leq 5$, where the Ziman formula gives a reasonable estimate of the plasmon damping at $k=0$. The question of plasmon damping and dispersion at very high coupling $r_s > 5$ is beyond the scope of this paper. Looking at the plasmon position (solid black curve), for $r_s < 2$, $\omega(k=0)$ follows the plasma frequency $\hbar\omega_{\rm pl}/E_F \propto \sqrt{r_s}$ (dashed black curve). At stronger coupling, Im $\nu(\omega_{\rm pl})$, and hence the plasmon position at $k=0$, increases. Again, in the

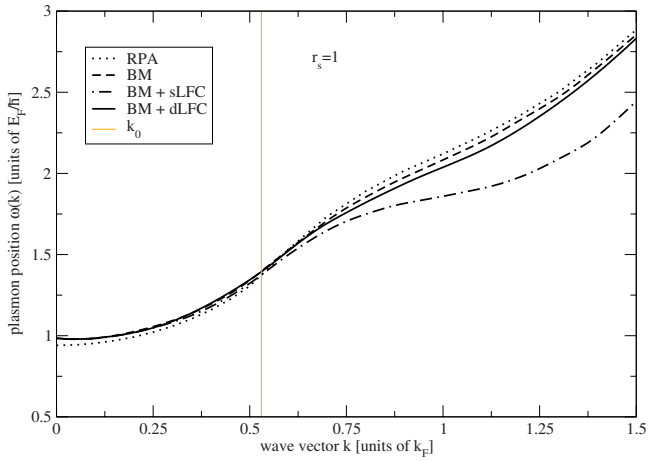

FIG. 6. (Color online) Plasmon shift $\omega(k)$ as a function of the wave vector k for $r_s=1$ BM: traditional Born-Mermin approximation. BM+sLFC: Born-Mermin including static local-field corrections. BM+dLFC: Born-Mermin including dynamic local-field corrections.

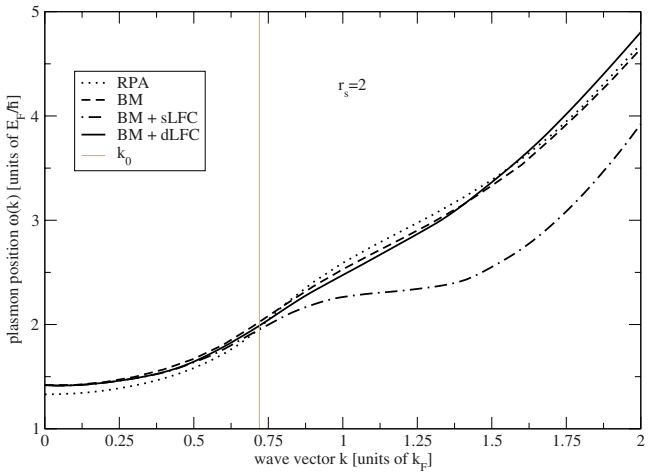

FIG. 7. (Color online) Plasmon shift $\omega(k)$ as a function of the wave vector k for $r_s=2$. BM: traditional Born-Mermin approximation. BM+sLFC: Born-Mermin including static local-field corrections. BM+dLFC: Born-Mermin including dynamic local-field corrections.

regime of moderate coupling, $r_s \gtrsim 2$, both real and imaginary part of the collision frequency contribute to the plasmon shift, which makes the discussion of r_s scaling difficult.

Interestingly, we observe, that plasmon damping and shift show different dependence on density, i.e., r_s. Taking into account that the Fermi energy scales as $1/r_s^2$, the plasmon damping is to lowest order independent of density, while the plasmon dispersion follows roughly the $\sqrt{r_s}$ behavior. The reason behind this difference is related to the fact that the plasmon collisional damping is a true many-body effect, not present in a model neglecting correlations. On the other hand, the plasmon dispersion is—to lowest order—already included in the mean-field theory or RPA. We will not dwell further on this subject here, however, a general remark should be made: To clarify the question of density dependence of quantities describing energy dissipation in interacting many-body systems requires in-depth analysis of the perturbative methods applied to their calculation. E.g., in the case of the single-particle self-energy, describing the dispersion and damping of single-particle excitations, it has been found, that a consistent density scaling can only be found in a generic nonperturbative calculation [42].

Next, we present the wave vector dependence of the plasmon shift $\omega(k)$ and the plasmon width $\Gamma(k)$. The results for the shift are shown in Figs. 6–8 for $r_s=1,2,5$. Figures 10–12 display the width for the same r_s values. We compare three different approximations, the traditional BM given by Eqs. (3) and (10), the extended Born-Mermin approach with static local-field correction (BM+sLFC) of Eq. (7), together with Eq. (13), and finally the extended Born-Mermin approach with dynamic local-field corrections (BM+dLFC) by the Dabrowski ansatz, i.e., Eqs. (19) and (22). Also, the RPA dispersion relation is shown, with $1-V(k)\chi^{(0)}[k,\omega(k)]=0$ for $k<k_0$ and the position of the maximum of Im $\chi_{ee}^{\mathrm{RPA}}(k,\omega)$ for $k>k_0$.

The shift at $k=0$ shown in these figures corresponds to the values for $r_s=1,2,5$ in Fig. 5. In this limit, the local-field corrections do not contribute. Thus, the different approximations (i.e., BM, BM+sLFC, and BM+dLFC) merge for $k \to 0$. As in the long-wavelength limit, the deviation of all approximative expressions from the RPA results are more pronounced with increasing r_s. As for the Born-Mermin result, it shows a systematic behavior with a switch from a blue shift to a red shift at a value of k close to k_0. Similar results have been reported by Thiele *et al.* [5], where calculations for finite temperature conditions at moderate degeneracy are given. We refer for details to that paper and take the traditional Born-Mermin results as a reference point for the inclusion of local-field effects.

Using the extended Born-Mermin approach together with a static local-field correction shows a drastic change in the dispersion relation for larger values of k. This is expected from Fig. 2, where $G_{ee}(k)$ shows considerable deviations

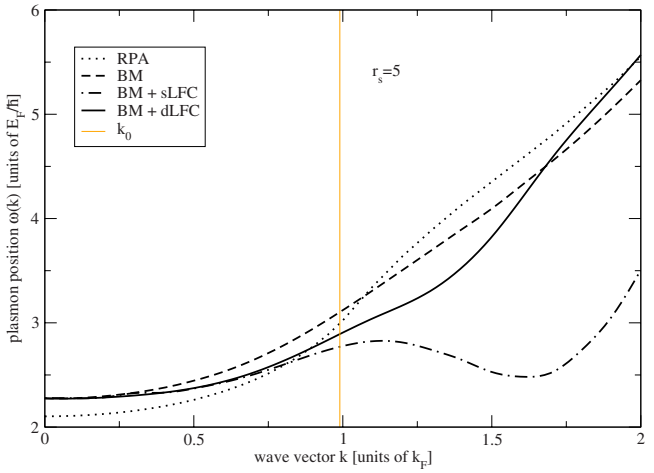

FIG. 8. (Color online) Plasmon shift $\omega(k)$ as a function of the wave vector k for $r_s=5$. BM: traditional Born-Mermin approximation. BM+sLFC: Born-Mermin including static local-field corrections. BM+dLFC: Born-Mermin including dynamic local-field corrections.

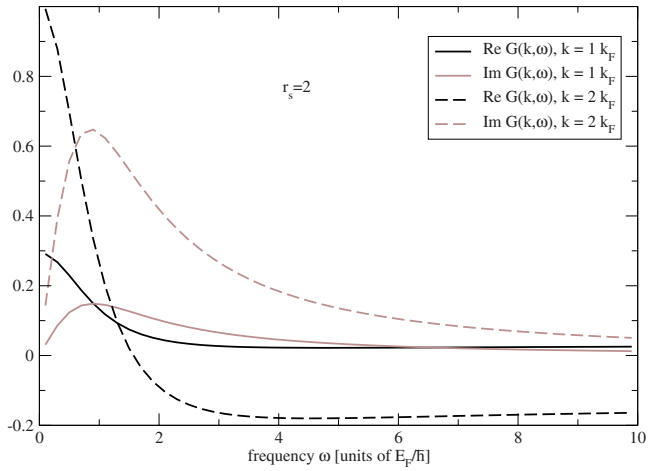

FIG. 9. (Color online) Real and imaginary part for dynamic local-field correction at $r_s=2$ for two different wave vectors as a function of the frequency.

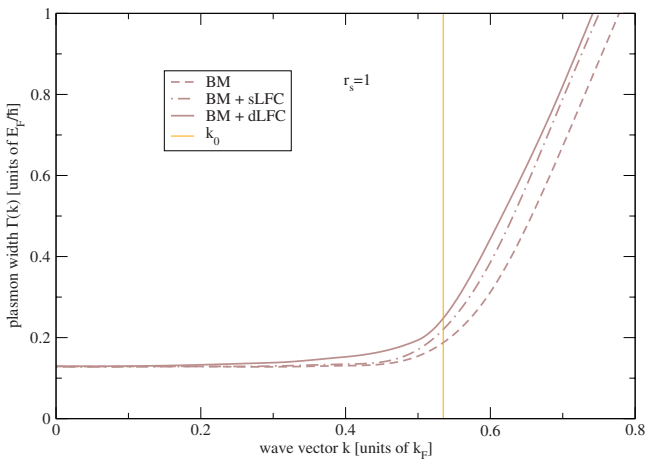

FIG. 10. (Color online) Plasmon width $\Gamma(k)$ as a function of the wave vector k for $r_s=1$. The traditional Born-Mermin (BM) without local-field corrections is compared to the extended approach with static (BM+sLFC) and dynamic local-field corrections (BM +dLFC). The onset k_0 of Landau damping in RPA is also shown.

from the RPA limit, i.e., $G_{ee}(k)=0$. Also, the larger local-field factor for increasing r_s leads to a more pronounced change in the dispersion relation, as can be seen by comparing the three values of r_s. However, once we refine the approximation by allowing for dynamic local-field corrections, these drastic changes disappear again and a dispersion close to the original Born-Mermin curve is found, at least for $r_s=1$ and $r_s=2$. In the case of $r_s=5$, noticeable differences from both, BM and BM+sLFC remain.

This behavior can be understood by inspection of the frequency dependence of Re $G_{ee}(k,\omega)$. While Re $G_{ee}(k,0)$ increases with k, Re $G_{ee}(k,\infty)$ is considerably smaller or even negative for large k, see, e.g., [37]. As a consequence, values at intermediate frequencies are considerable smaller than the static value Re $G_{ee}(k,0)$. For larger values of k, a zero in Re $G_{ee}(k,\omega)$ is found corresponding to a RPA-like behavior at this frequency.

We illustrate this fact in Fig. 9, showing the real and the imaginary part of the dynamic local-field correction as a function of the frequency ω for $k=k_F$, $k=2k_F$ and $r_s=2$. At $\omega=0$, the real part of the dynamical LFC is fixed by construction through the Farid approximation, scaling as k^2 in the long-wavelength limit. At $\omega\to\infty$, the high-frequency limit applies, cf. Eq. (16). This limits also scales as k^2 for $k\to 0$. Details are presented in the Appendix. Due to the Padé ansatz in Eq. (19), the imaginary part starts linearly for small ω, while the high-frequency behavior is given by the perturbative result. In between there is a maximum whose position is at $\omega_{\max}=\sqrt{2/3b(k)}$, with Im $G_{ee}(k,\omega_{\max})=(3/5)^{5/4}a(k)/\sqrt{3b(k)/2}$, see the Appendix for a detailed analysis. In the long-wavelength limit, one observes $a(k)\propto k^2$ and $b(k)\propto k^0$. Even at finite k, a careful analysis shows that $b(k)$ and in turn $\omega_{\max}$ only weakly depend on k. Also, the amplitude scales as k^2, which explains the behavior of the two dashed curves in Fig. 9, i.e., comparing the cases $k=k_F$ and $k=2k_F$. As for the solid lines, the real and imaginary part are connected by a Kramers-Kronig relation. Thus, Re $G_{ee}(k,\omega)$ shows a small value or a zero at the position where the maximum occurs in Im $G_{ee}(k,\omega)$.

Note, however, that the dispersion relation given for the calculations including the dynamical LFC is somewhat misleading. A frequency scan of the dynamic structure factor reveals a rich structure, which cannot be adequately represented by a shift and a width only.

Finally, we investigate the plasmon width at $r_s=1$, 2, and 5 for the three different approximations, see Figs. 10–12. Again, at $k=0$, the broadening is only due to the collision frequency. For $k>k_0$, the rapid increase of the broadening with k is due to Landau damping. At finite k, local-field effects also contribute. In particular, the imaginary part of the dynamic local-field correction adds to the total width of the plasmon, if one compares the BM+dLFC result to the BM curve. To first order, the additional damping due to the imaginary part of the LFC can be estimated as $\Delta\Gamma(k)\simeq 2$ Im $G_{ee}[k,\omega(k)]\omega(k)$. Taking the values at $r_s=2$ and k

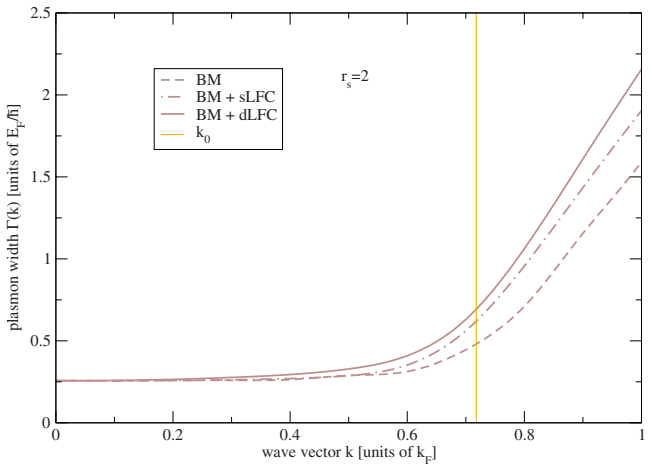

FIG. 11. (Color online) Plasmon width $\Gamma(k)$ as a function of the wave vector k for $r_s=2$. BM: traditional Born-Mermin approximation. BM+sLFC: Born-Mermin including static local-field corrections. BM+dLFC: Born-Mermin including dynamic local-field corrections.

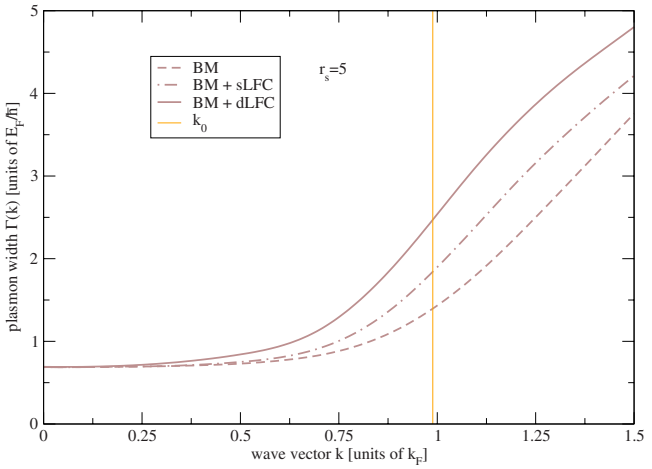

FIG. 12. (Color online) Plasmon width $\Gamma(k)$ as a function of the wave vector k for $r_s=5$. BM: traditional Born-Mermin approximation. BM+sLFC: Born-Mermin including static local-field corrections. BM+dLFC: Born-Mermin including dynamic local-field corrections.

$=k_F$, where $\omega(k_F)\simeq 2.5E_F/\hbar$, we find $\Delta\Gamma(k_F)\simeq 0.7E_F/\hbar$, which agrees with the values in Fig. 11.

Although the static LFC is real valued, it gives a change to the plasmon width as well. This is due to the frequency dependence of the collision frequency. Taking the static LFC into account, the plasmon position is shifted to lower energies as compared to RPA, and hence the plasmon is stronger damped, owing to the increased collision frequency at the lowered plasmon energy. For illustration, we consider again the case $r_s=2$: At $k=k_F$, the plasmon position in the Born-Mermin and in the Born-Mermin plus static LFC approximations are, respectively, $\omega_{\mathrm{BM}}(k_F)\simeq 2.5E_F/\hbar$ and $\omega_{\mathrm{BM+sLFC}}(k_F)\simeq 2.3E_F/\hbar$, cf. Figure 7. Using the well-known [22] high-frequency behavior Re $\nu(\omega)\propto\omega^{-3/2}$ for the collision frequency, we can estimate the ratio of damping in both models as $\Gamma_{\mathrm{BM}}/\Gamma_{\mathrm{BM+sLFC}}\simeq\nu(\omega_{\mathrm{BM}}(k_F))/\nu(\omega_{\mathrm{BM+sLFC}}(k_F))\simeq(\omega_{\mathrm{BM+sLFC}}(k_F)/\omega_{\mathrm{BM}}(k_F))^{3/2}=(2.3/2.5)^{3/2}=0.88$. This estimate agrees well with the values for $\Gamma(k_F)$ in Born-Mermin approximation and using the extended model with static LFC at $r_s=2$, see Fig. 11.

It remains to point out that for both functions, plasmon shift and position, the deviation between various models becomes stronger as r_s increases and at $k\simeq k_0$, the onset of Landau damping. This is an important information for experimental studies of cold solid density plasmas. As long as $r_s<2$, i.e., in the weakly coupled regime, scattering at k vectors up to k_0 allows for robust determination of plasma density, temperature, and transport coefficients by measuring the plasmon dispersion and damping, since the models agree within typical accuracy of x-ray plasma scattering experiments. At increased r_s, the range of k vectors where models agree is confined to lower k, e.g., $k<0.5k_0$ in the case $r_s=5$.

So far, we have only presented results using the adapted Dabrowski ansatz for the dynamical local-field correction of the electron gas. The overall behavior of the plasmon dispersion with a recurrence-relation based approach outlined above, cf. Eq. (23) and (24), is similar, while there are notable differences in detail. This is in part due to fundamental differences in the high-frequency behavior of the imaginary part of the local-field factor. We will discuss this in a forthcoming paper.

V. CONCLUSIONS

We devise an extended Mermin approach which incorporates both, electron-ion collisions as well as electron-electron correlations. We apply this new formalism to the calculation of the dynamical structure factor for an interacting electron gas at $T=0$ interacting with a background of inert ions. As inputs act a dynamical collision frequency taken in Born approximation and various models for dynamic local-field corrections of the interacting OCP electron gas. Being important experimental observables, we focus on the spectral properties of plasmon resonances in the structure factor, and we analyze the relevance of collisions and correlations on these signatures.

At small wave vectors, we observe a dominance of collisions. The importance of local-field corrections increase with increasing Brueckner parameter r_s. For $r_s=5$, it is indispensable to account for local-field correlations. Drastic changes in the plasmon properties which occur by taking account of static local-field corrections disappear to some extent when using models for dynamic local-field corrections. The plasmon broadening shows in general a very involved behavior, due to the interplay between dynamical collision frequency and static or dynamic LFC. In the case of static LFC, the ratio of plasmon damping in BM and BM+sLFC approximations can be estimated as $\nu[\omega_{\mathrm{BM}}(k)]/\nu[\omega_{\mathrm{BM+sLFC}}(k)]\simeq[\omega_{\mathrm{BM+sLFC}}(k)/\omega_{\mathrm{BM}}(k)]^{3/2}$. Using the dynamical LFC, the additional damping due to the imaginary part of the LFC is $\Delta\Gamma(k)\simeq 2\ \mathrm{Im}\ G_{ee}[k,\omega(k)]\omega(k)$.

Recently, x-ray Thomson scattering (XRTS) has been successful in characterizing warm dense matter. To analyze the scattering data, the conventional Born-Mermin approximation has been used. The extended Mermin approach presented in this work allows the application of the XRTS technique also to dense plasmas at temperatures far below the Fermi temperature, i.e., to degenerate, yet strongly coupled plasmas. The experimental determination of the plasmon dispersion and damping in such systems via XRTS seems a highly promising project, since, together with the existing data for hot plasmas and warm dense matter, it allows to study the thermodynamic, structural, and dynamical properties of matter under extreme conditions and their changes over a broad range of plasma parameters using the identical technique and a unified theoretical approach.

The presented results show that the plasmon width and the plasmon shift calculated with various models for the local-field factor agree to a certain extend as long as $r_s\leq 2$, i.e., in the weak coupling regime. Thus, scattering experiments with $r_s<2$ plasmas allow for robust determination of plasma parameters and transport coefficients via fitting model structure factors. At $r_s>2$, these models start to deviate significantly. Agreement is only observed at extreme forward scattering $k<0.5k_F$, where plasmons are difficult to probe due to the increased elastic scattering component and smaller plasmon shift.

The presented formalism can also serve as a tool to study the interplay of impurity scattering and electron-electron correlations in a jellium model description of metals. Here, connection can be made to experimental results for the dynamic structure factor measured by inelastic x-ray scattering [43].

ACKNOWLEDGMENTS

This work was supported by the Deutsche Forschungsgemeinschaft (DFG) within the Grant No. Sonderforschungsbereich SFB 652. C.F. also acknowledges support by the Alexander von Humboldt-Foundation. All authors thank the anonymous referee for many helpful comments and suggestions. We are furthermore indebted to S. Glenzer and P. Neumayer for pointing us toward the problems presented in this article.

APPENDIX: ANALYSIS OF THE DYNAMICAL LFC

Of course, the shape of the imaginary part as well as the real part of the dynamic local-field correction $G_{ee}(k,\omega)$ depends crucially on the ansatz made by Dabrowski for the imaginary part. The real part is then obtained from the Kramers-Kronig relation. The Padé approximant of Dabrowski reads, see Eq. (19),

$$\mathrm{Im}\, G_{ee}(k,\omega) = \frac{a(k)\omega}{(1+b(k)\omega^2)^{5/4}}. \tag{A1}$$

Taking the derivative, we obtain

$$\frac{d\,\mathrm{Im}\, G_{ee}(k,\omega)}{d\omega} = \frac{a(k)(2-3b(k)\omega^2)}{2(1+b(k)\omega^2)^{9/4}}. \tag{A2}$$

Thus, the maximum position for the imaginary part is given by

$$\omega_{\max} = \sqrt{\frac{2}{3b(k)}} \tag{A3}$$

As for the value at the maximum position, we have

$$\mathrm{Im}\, G_{ee}(k,\omega_{\max}) = \left(\frac{3}{5}\right)^{5/4} \sqrt{\frac{2}{3}} \frac{a(k)}{\sqrt{b(k)}}. \tag{A4}$$

Now, $b(k)$ and $a(k)$ are defined by Eq. (20). In the long-wavelength limit, both $\mathrm{Re}\, G_{ee}(k,0)$ and $\mathrm{Re}\, G_{ee}(k,\infty)$ scale as k^2. The detailed behavior was analyzed, e.g., by Iwamoto [44] to read,

$$\lim_{k\to 0} \mathrm{Re}\, G_{ee}(k,0) = \gamma(r_s)\left(\frac{k}{k_F}\right)^2, \tag{A5}$$

$$\lim_{k\to 0} \mathrm{Re}\, G_{ee}(k,\infty) = \left(\frac{3}{20} + \frac{11}{20}\pi\alpha r_s E_c + \frac{13}{20}\pi\alpha r_s^2 \frac{dE_c}{dr_s}\right)\left(\frac{k}{k_F}\right)^2, \tag{A6}$$

with

$$\gamma(r_s) = \frac{1}{4} - \frac{\pi\alpha r_s^5}{24}\frac{d}{dr_s}\left(\frac{1}{r_s^2}\frac{dE_c}{dr_s}\right). \tag{A7}$$

Here, the correlation energy $E_c(r_s)$ enters. This quantity can be taken from well elaborated fitting formulas, see Refs. [41,45]. In particular, the small r_s, i.e., high density limit allows for simple analytic approximations of $E_c(r_s)$, see again Ref. [44],

$$E_c = \frac{2}{\pi^2}(1-\ln 2)\ln r_s - 0.094 + 0.018 r_s \ln r_s + O(r_s). \tag{A8}$$

As a consequence of the scaling of $\mathrm{Re}\, G_{ee}(k,0)$ and $\mathrm{Re}\, G_{ee}(k,\infty)$ with k^2, the coefficient $b(k)$ behaves as k^0 and $a(k)$ as k^2. In turn, $\mathrm{Im}\, G_{ee}(k,\omega_{\max})$ is proportional to k^2 in accordance to the discussion given above. In particular, for $r_s \ll 1$, we obtain from Eq. (A8),

$$\begin{aligned}\lim_{k\to 0}[CDb(k)]^{3/4} = {} & \frac{1}{10} - \frac{11}{10\pi}(1-\ln 2)\alpha r_s \ln r_s \\ & + \left[\frac{11\pi}{20}0.094 - \frac{21}{20\pi}(1-\ln 2)\right]\alpha r_s \\ & - \frac{67}{60}\pi\alpha 0.018 r_s^2 \ln r_s - \frac{73}{120}\pi\alpha 0.018 r_s^2.\end{aligned} \tag{A9}$$

[1] S. H. Glenzer and R. Redmer, Rev. Mod. Phys. **81**, 1625 (2009).
[2] S. H. Glenzer, G. Gregori, R. W. Lee, F. J. Rogers, S. W. Pollaine, and O. L. Landen, Phys. Rev. Lett. **90**, 175002 (2003).
[3] A. Höll, R. Redmer, G. Röpke, and H. Reinholz, Eur. Phys. J. D **29**, 159 (2004).
[4] S. H. Glenzer, O. L. Landen, P. Neumayer, R. W. Lee, K. Widmann, S. W. Pollaine, R. J. Wallace, G. Gregori, A. Höll, T. Bornath, R. Thiele, V. Schwarz, W.-D. Kraeft, and R. Redmer, Phys. Rev. Lett. **98**, 065002 (2007).
[5] R. Thiele, T. Bornath, C. Fortmann, A. Höll, R. Redmer, H. Reinholz, G. Röpke, A. Wierling, S. H. Glenzer, and G. Gregori, Phys. Rev. E **78**, 026411 (2008).
[6] J. Chihara, J. Phys. F: Met. Phys. **17**, 295 (1987).
[7] G. Gregori, S. H. Glenzer, W. Rozmus, R. W. Lee, and O. L. Landen, Phys. Rev. E **67**, 026412 (2003).
[8] S. Ichimaru, Rev. Mod. Phys. **54**, 1017 (1982).
[9] O. L. Landen, S. H. Glenzer, M. J. Edwards, R. W. Lee, G. W. Collins, R. C. Cauble, W. W. Hsing, and B. A. Hammel, J. Quant. Spectrosc. Radiat. Transf. **71**, 465 (2001).
[10] A. Höll *et al.*, Proc. R. Soc. A **3**, 120 (2007).
[11] N. D. Mermin, Phys. Rev. B **1**, 2362 (1970).
[12] C. Fortmann, T. Bornath, R. Redmer, H. Reinholz, G. Röpke,

V. Schwarz, and R. Thiele, Laser Part. Beams **27**, 311 (2009).
[13] J. Hubbard, Proc. R. Soc. London, Ser. A **243**, 336 (1957).
[14] A. Wierling, J. Phys. A: Math. Theor. **42**, 214051 (2009).
[15] D. Zubarev, V. Morozov, and G. Röpke, *Statistical Mechanics of Nonequilibrium Processes* (Akademie-Verlag, Berlin, 1997), Vol. 2.
[16] G. Röpke, A. Selchow, A. Wierling, and H. Reinholz, Phys. Lett. A **260**, 365 (1999).
[17] G. Gregori, S. H. Glenzer, and O. L. Landen, J. Phys. A **36**, 5971 (2003).
[18] G. Gregori, A. Ravasio, A. Höll, S. H. Glenzer, and S. J. Rose, High Energy Density Phys. **3**, 99 (2007).
[19] S. Ichimaru, S. Mitake, S. Tanaka, and X.-Z. Yan, Phys. Rev. A **32**, 1768 (1985).
[20] J. Daligault and M. S. Murillo, Phys. Rev. E **68**, 015401(R) (2003).
[21] S. V. Adamjan, I. M. Tkachenko, J. L. Munoz-Cobo Gonzalez, and G. Verdu Martin, Phys. Rev. E **48**, 2067 (1993).
[22] G. Röpke, R. Redmer, A. Wierling, and H. Reinholz, Phys. Rev. E **60**, R2484 (1999).
[23] H. Reinholz, R. Redmer, G. Röpke, and A. Wierling, Phys. Rev. E **62**, 5648 (2000).
[24] N. R. Arista and W. Brandt, Phys. Rev. A **29**, 1471 (1984).
[25] M. D. Barriga-Carrasco, Phys. Rev. E **79**, 027401 (2009).
[26] K. Utsumi and S. Ichimaru, Phys. Rev. B **22**, 5203 (1980).
[27] B. Farid, V. Heine, G. E. Engel, and I. J. Robertson, Phys. Rev. B **48**, 11602 (1993).
[28] S. Ichimaru, *Statistical Plasma Physics* (Addison-Wesley, Reading, MA, 1994), Vol. II.
[29] E. Engel and S. H. Vosko, Phys. Rev. B **42**, 4940 (1990).
[30] K. Singwi, M. P. Tosi, R. H. Land, and A. Sjölander, Phys. Rev. **176**, 589 (1968).
[31] S. Moroni, D. M. Ceperley, and G. Senatore, Phys. Rev. Lett. **75**, 689 (1995).
[32] A. Holas, in *Strongly Coupled Plasma Physics*, edited by F. J. Rogers and H. E. DeWitt (Plenum, New York, 1987).
[33] B. Dabrowski, Phys. Rev. B **34**, 4989 (1986).
[34] J. Hong and M. H. Lee, Phys. Rev. Lett. **55**, 2375 (1985).
[35] C. F. Richardson and N. W. Ashcroft, Phys. Rev. B **50**, 8170 (1994).
[36] M. H. Lee and J. Hong, J. Phys.: Condens. Matter **1**, 3867 (1989).
[37] N. Iwamoto, E. Krotscheck, and D. Pines, Phys. Rev. B **29**, 3936 (1984).
[38] A. J. Glick and W. F. Long, Phys. Rev. B **4**, 3455 (1971).
[39] E. K. U. Gross and W. Kohn, Phys. Rev. Lett. **55**, 2850 (1985).
[40] In difference to Ref. [34], a factor of z has been included into the definition of c_2^0. Furthermore, $-iz$ is used instead of z.
[41] P. Gori-Giorgi, F. Sacchetti, and G. B. Bachelet, Phys. Rev. B **61**, 7353 (2000).
[42] C. Fortmann, J. Phys. A **41**, 445501 (2008); Phys. Rev. E **79**, 016404 (2009).
[43] Early works are, e.g., P. M. Platzman and P. Eisenberger, Phys. Rev. Lett. **33**, 152 (1974); P. E. Batson and J. Silcox, Phys. Rev. B **27**, 5224 (1983); For a recent review, see W. Schülke, J. Phys.: Condens. Matter **13**, 7557 (2001).
[44] N. Iwamoto, Phys. Rev. A **30**, 3289 (1984).
[45] S. H. Vosko, L. Wilk, and M. Nusair, Can. J. Phys. **58**, 1200 (1980); J. P. Perdew and Y. Wang, Phys. Rev. B **45**, 13244 (1992); E. Proynov and J. Kong, Phys. Rev. A **79**, 014103 (2009).